A second-generation superconducting undulator cryostat for the APS

IOP Conf. Series: Materials Science and Engineering **278** (2017) 012176 doi:10.1088/1757-899X/278/1/012176

A second-generation superconducting undulator cryostat for the APS

J Fuerst, Q Hasse, Y Ivanyushenkov, M Kasa and Y Shiroyanagi

Argonne National Laboratory, Argonne, IL 60439, USA

E-mail: fuerst@anl.gov

Abstract. A second-generation cryocooler-based cryostat has been designed and built to support a new helically wound superconducting undulator (SCU) magnet for the Advanced Photon Source (APS) at Argonne National Laboratory (ANL). The design represents an evolution of existing SCU cryostats currently in operation in the APS storage ring. Value engineering and lessons learned have resulted in a smaller, cheaper, and simpler cryostat design compatible with existing planar magnets as well as the new helically wound device. We describe heat load and quench response results, design and operational details, and the "build-to-spec" procurement strategy.

1. Introduction

The APS is a third-generation storage ring synchrotron light source. It consists of a seven giga-electron-volt (GeV) electron storage ring (SR) combined with multiple x-ray beam lines using both bending magnet (BM) and insertion device (ID) sources capable of delivering photons in the hard x-ray energy spectrum. Figure 1 shows one sector of the SR with an ID source identified.

In recent years two new undulator IDs using superconducting magnet technology have been deployed in the SR [1,2]. These devices demonstrate enhanced performance compared with conventional permanent-magnet IDs due to higher operational magnetic fields. The cryostat design for these first-generation superconducting undulators is based on superconducting wiggler IDs developed at the Budker Institute of Nuclear Physics (BINP) in Novisibirsk [3]. Refrigeration is supplied using cryocoolers operating at three different temperature levels in a reliable, low-maintenance configuration. Lessons learned from several years of operation guided design modifications which have been implemented in a second-generation cryostat providing increased installation versatility, simplified assembly, and reduced production cost.

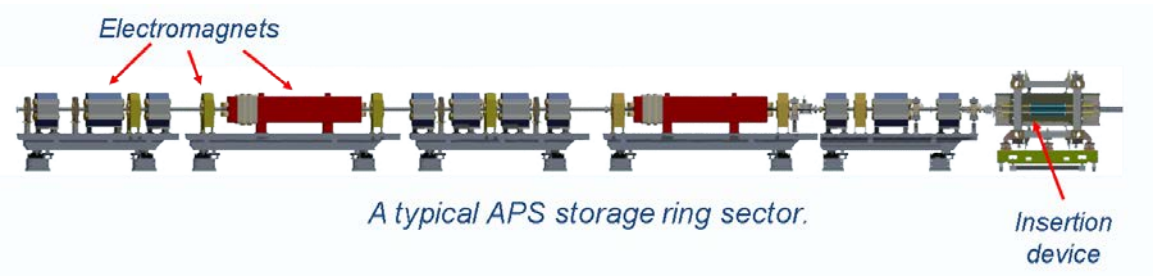

Figure 1. APS SR sector showing ID location on the right (permanent magnet ID shown).

2. Design evolution

Many lessons were learned from the operating experience gained with the first generation SCUs. In addition to meeting the design specifications for magnetic field strength and quality, the devices demonstrated zero-boil-off operation at the design operating temperature. Goals for the second generation cryostat included reduced production cost, simplified assembly and a smaller physical envelope to enable more flexible installation options in the APS SR while maintaining zero-boil-off operation. At the same time many features of the BINP design are retained. The basic cooling strategy using cryocoolers to re-liquefy helium by chilling the exterior of a small storage reservoir works well although the reservoir volume has been reduced from 100 L to 30 L. This contributes to a reduction in cryostat diameter (0.5 m compared to 0.9 m), a design goal which is also aided by changes to the cold mass layout and the thermal shield design. Figure 2 shows a CAD model of the new design.

The new design uses an integrated 4.2 K cold mass layout where the magnet is attached directly to the underside of the helium reservoir via end brackets. Also a single thermal shield operating at 35 K is used instead of two shields. Finally, the first-generation design's cryocooler layout (two 4.2 K units plus two 20 K units) is replaced by four 4.2 K cryocoolers and a single thermal shield. The proposed changes were supported by numerical analyses [4] which predict an overall increase in excess cryocooler capacity at 4.2 K in addition to the benefits of reduced complexity and cost.

Value engineering was used to selectively re-design certain subsystems to reduce cost. The overall reduction in cryostat diameter allows the use of standard ISO NW500 flanges for the cryostat ends rather than custom dished heads. The magnet current lead turret designs were modified to reduce part count and simplify assembly while the helium fill and vent/relief functions were separated into distinct spool pieces, reducing complexity and easing assembly. Figure 3 shows an exploded view of the cryostat assembly.

A design/build procurement strategy was pursued for the cryostat primary component package (vacuum vessel, thermal shield and LHe reservoir) in an effort to further reduce cost and improve schedule. Significant cost savings were realized by providing CAD models and a detailed scope of work/technical specification which were used by the vendor to produce production drawings and (following ANL approval) cryostat components. This is in contrast to the first-generation cryostat build-to-print procurement strategy for the same component set which involved in-house production of a complete fabrication drawing package.

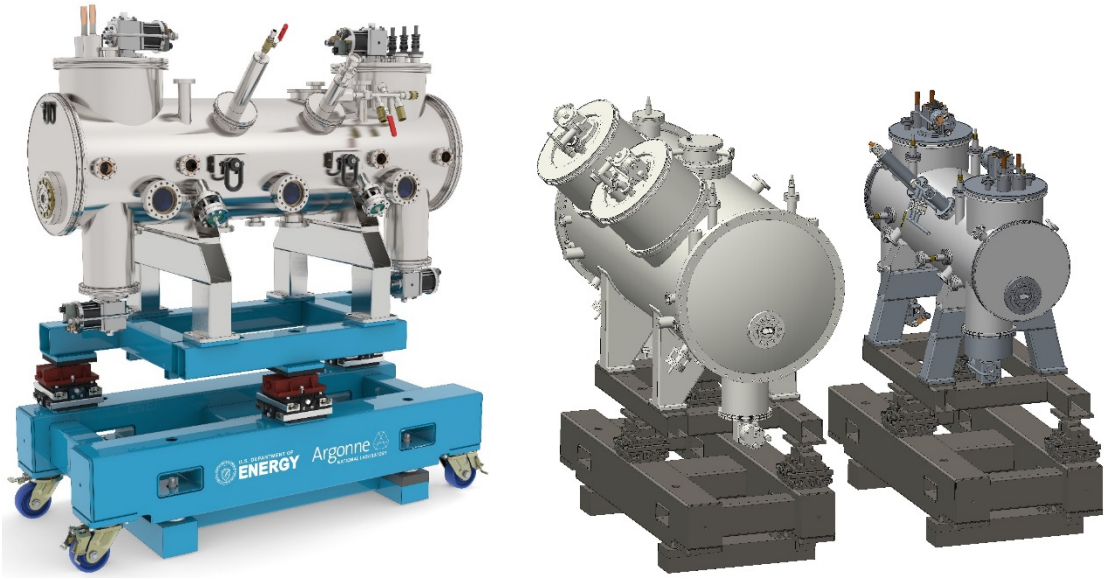

a **b**

Figure 2. CAD models of second-generation cryostat (a) and comparison with original design (b).

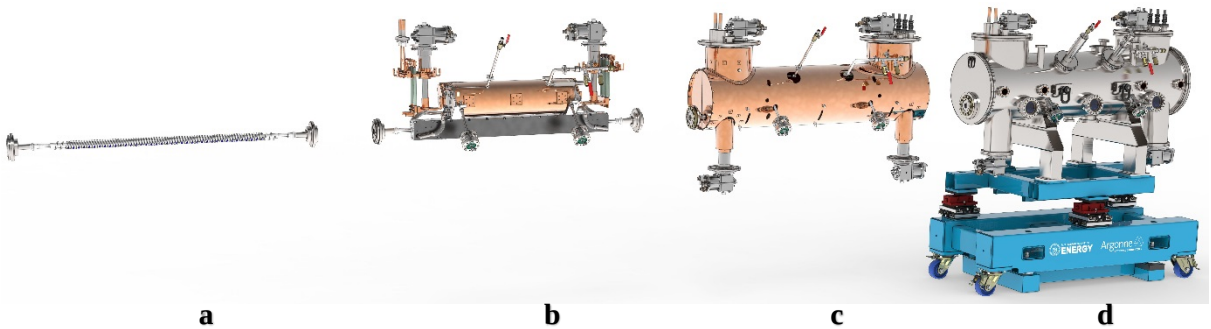

Figure 3. Exploded view of the cryostat showing magnet/beam chamber (a), 4.2 K cold mass (b), cold mass with thermal shield (c), and complete assembly (d).

3. Cryostat execution and operational performance

The new design was meant to be less expensive, faster to fabricate, easier to assemble, and smaller in size compared to the original design while at the same time providing equal or better performance. For the most part these goals have been achieved although meeting the performance target has required several engineering runs (not including the magnet core) to shake down the assembly sequence and reduce the static heat load. At present the cryostat is in final acceptance tests and will be ready for final assembly with the completed magnet in late summer 2017.

3.1. Execution

The complete cryostat assembly including all subsystems was modeled in PTC Creo Parametric 3.0 over a six-month period. All part features were represented sufficient to describe the design although some information (tolerances, surface finishes) were not included. For the main cryostat components (vacuum vessel, thermal shield, and LHe reservoir,) a companion scope of work/technical specification document was written to provide the missing information and establish global tolerances, finishes, and production techniques where appropriate. Inspection and test requirements including leak checking were also included. This document together with the relevant CAD data (in .stp file format) was competitively bid and awarded in the fall of 2016. The award contract included as a deliverable the creation of detail drawing packages for each major component. Drawings were submitted, iterated upon, and approved prior to fabrication start. The total elapsed time for fabrication and acceptance of these components was less than six months including the detail drawing production. The equivalent components for the first generation cryostat required about the same time to fabricate in addition to substantial in-house design/detailing effort. The final product was accepted with a few minor modifications required as well as some minor updates to the delivered drawing package.

The remaining subsystem components (including cryocooler/current lead turrets, support & alignment systems, magnet, beam vacuum chamber) were detailed in-house and produced in parallel with the main component contract. Value engineering of several of these ancillary subsystems reduced part count and yielded simpler, more easily assembled components. The cryostat was ready for cold tests without the magnet by late February 2017. Figure 4 shows pictures of selected subsystem component assemblies.

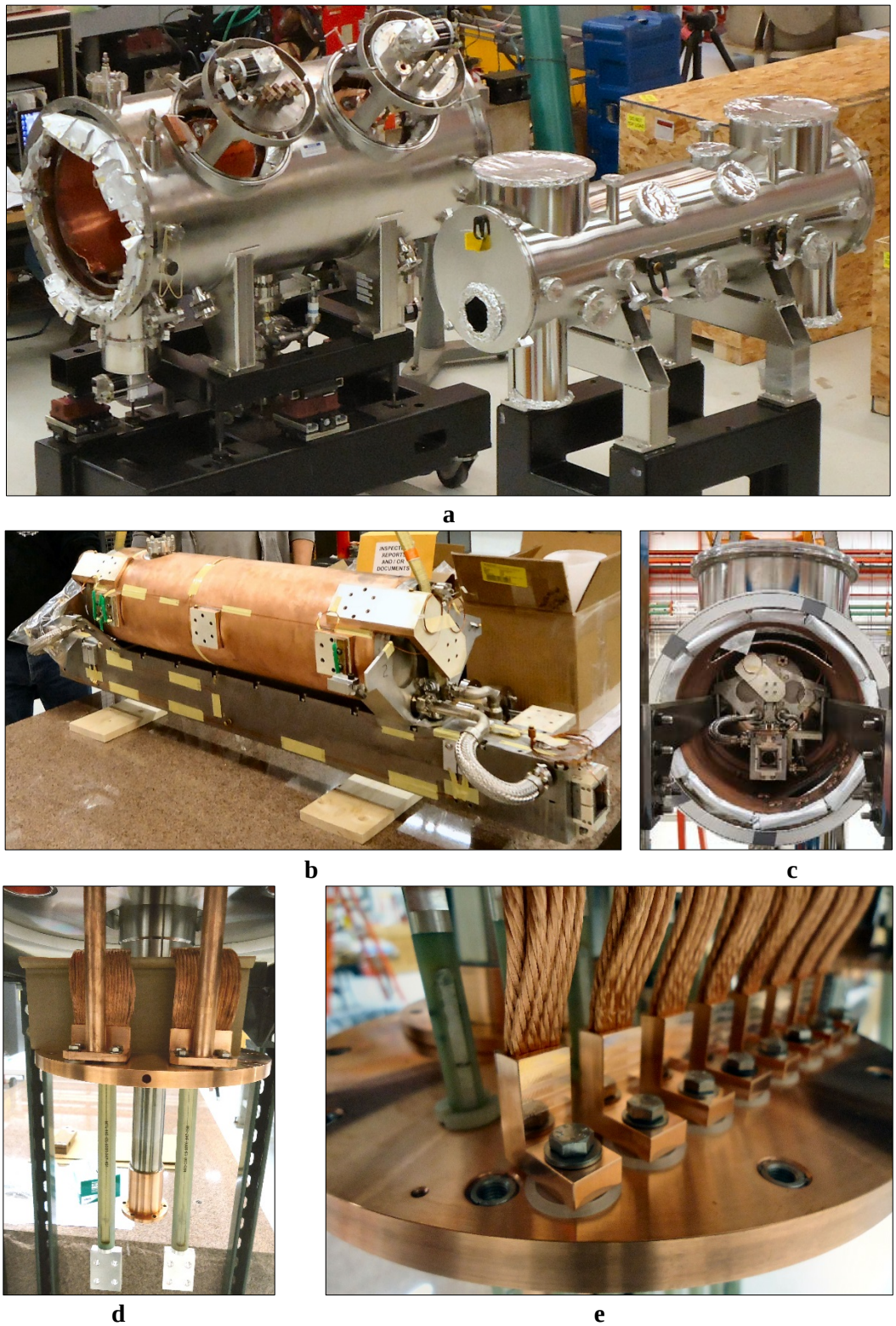

Figure 4. Cryostat vacuum vessel next to the first-generation SCU cryostat (a); cold mass assembly including magnet potting mold/strongback (b); end view of cold mass loaded into cryostat (c); main current lead assembly showing normal and high-temperature superconductor (HTS) leads with cryocooler in the background (d); corrector current lead assembly showing thermal connection detail between normal conducting (braid) lead and cryocooler first stage (e).

3.2. Operational performance

The complete cryostat assembly (without magnet) was thermal cycled six times between March and June 2017 to evaluate cryogenic performance and implement necessary corrections. This substantial commissioning/test window was made possible by the timely delivery and acceptance of the cryostat components and took place while magnet development, fabrication and testing were underway.

The initial cooldowns established a cooldown time of about thirty hours compared to seventy hours required for the first generation design where cooldown time is driven by the 4 K cold mass. Both designs use high-conductance thermal links between the upper 4 K cryocoolers and the LHe reservoir. However in the first generation design, the magnets themselves are connected to the refrigeration source only by the tubes that join the magnet cooling channels to the LHe reservoir. The thermal contact is strong when LHe is present but weak otherwise, resulting in a slow magnet cooldown and the subsequent seventy hour cooldown time. The new design connects the additional two 4 K cryocoolers (which substitute for the two 20 K units in the original) directly to the magnet/potting mold greatly enhancing the thermal contact during cooldown. As a result cooldown takes half the time for similar cold mass cooldown enthalpies. Figure 5 shows the cooldown curve.

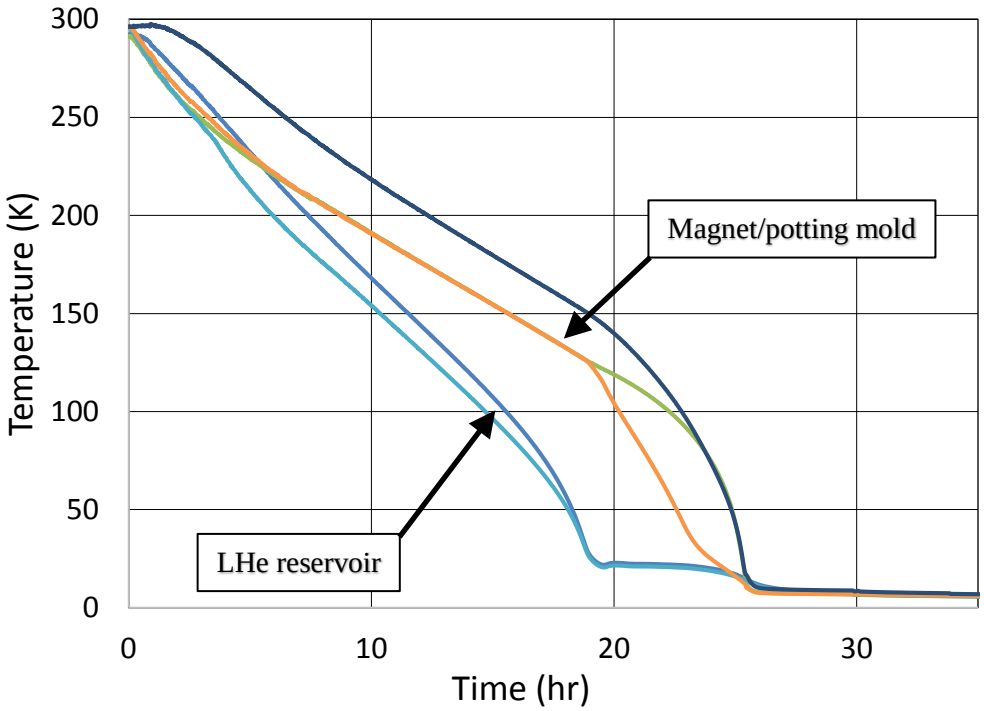

Figure 5. Cooldown curves showing cooling rates for selected temperature sensors on the LHe reservoir and the magnet/potting mold assembly. Once temperatures reach the 5 K range, LHe is transferred to the reservoir to complete the cooldown process.

Zero boil-off operation requires some amount of excess cooling capacity at the SCU operating temperature of 4.2 K. Since cryocooler refrigeration power depends on the equilibrium temperature reached by the system for a given heat load, a trim heater is used to equalize the total 4.2 K heat load with the available refrigeration. To reach the LHe reservoir operating temperature of 4.2 K, the base temperatures of the cryocooler second stages must operate at about 3.6 K due to thermal link conductances, contact resistances, and LHe re-condensation efficiency in the reservoir. Cryocooler load mapping indicates a per-unit cooling power of about 0.7 W at 3.6 K, suggesting a total available cooling power of 2.8 W with a 4.2 K LHe temperature. The system static heat load is estimated at about 1.3 W.

Initial cooldown reached only 5-7 K at the reservoir and magnet, respectively. During operation it was noticed that the lower cryocoolers had reached 2.7 K, indicating that they were providing negligible cooling power. Upper cryocoolers plateaued at the expected 3.6 K. Investigation after warmup revealed gaps in the radiation shield which, when analysed, accounted for a large fraction of the excess heat load beyond the approximately 1.5 W of available refrigeration and the resulting elevated equilibrium temperature. Follow-on cooldown/warmup cycles addressed both the higher-than-expected heat load and the lower-than-expected cooling power. The former was dealt with by a combination of improved assembly technique and a re-design of the cold mass thermal support system while the latter was traced to high-impedance conduction paths between the lower cryocoolers and the magnet/potting mold.

The magnet core and potting mold are both fabricated from 1026 steel. An aluminium mold had been considered early in the design phase, but concerns about differential thermal contraction resulted in the choice of 1026 steel to match the core. Unfortunately the relatively poor thermal conductivity of 1026 steel makes it challenging to extract heat with the required small (~0.2 K) temperature drop across the thermal path between the magnet and lower cryocoolers. Effective cooldown performance does not require such a small temperature drop but at operating temperature it is important. Initial tests indicated an almost 1.5 K temperature difference between the liquid helium temperature in the mold's cooling channels and the lower cryocooler second-stage temperatures.

Analysis indicates that an aluminium mold would solve this issue and plans exist to use such a mold in the assembly of a future developmental HSCU magnet. At present it should be possible to thermally engage the lower cryocoolers directly to the LHe reservoir using high-conductance copper bus in a manner similar to the upper cryocoolers. The performance price for this choice will be longer cooldown time (similar to the first generation design) due to the removal of direct thermal linkage between the lower cryocoolers and the massive magnet/potting mold assembly. The opportunity to explore cryogen-free "dry" operation is also sacrificed. Nevertheless this is a straightforward choice given the requirement to provide excess cooling power. A "lengthy" cooldown time is operationally acceptable.

Cryostat testing also included studies of system response to a simulated magnet quench. In operation the HSCU magnet is expected to release about seven kJ of stored energy to the system on a quench. Heaters mounted to the potting mold deliver this energy over about ten seconds – sufficient to replicate the long-term system response although the peak pressure in the LHe reservoir was somewhat less than estimated. Figure 6 shows the pressure and temperature response to the simulated quench. Further efforts to reduce heat load and increase cooling power will shorten the recovery time.

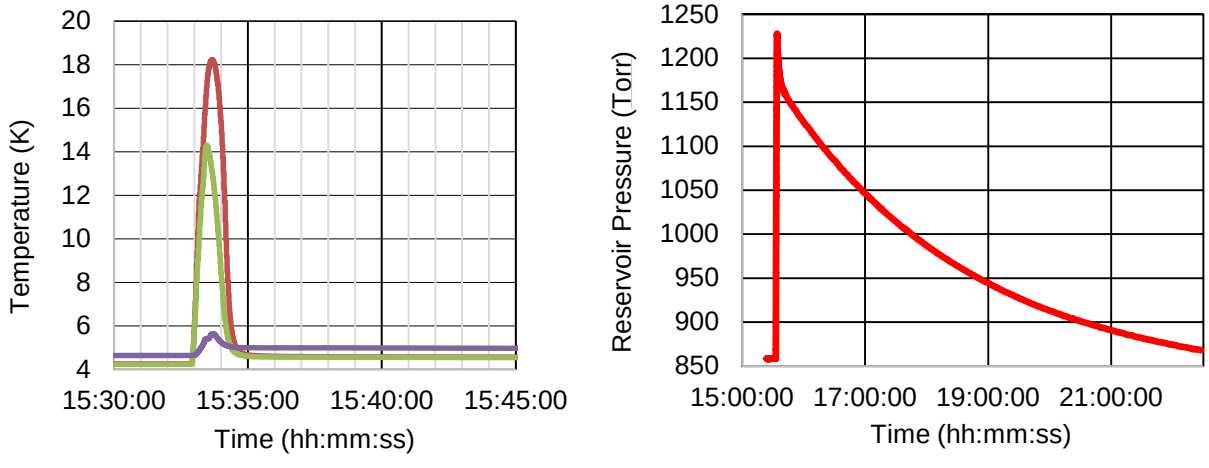

a **b**

Figure 6. System temperature (a) and pressure (b) response to a simulated seven kJ magnet quench event. System equilibrium pressure prior to the event was about 850 Torr. The initial pressure peak represents superheated vapor generated by the large heat flux. This vapour soon equilibrates back to saturated conditions, after which the heat is slowly removed using the excess cooling power of the system. The system did not vent helium during this event.

4. Conclusion

A new superconducting undulator cryostat has been developed based on lessons learned from devices currently in service at the APS. Design goals were to reduce cost by designing a smaller, simpler cryostat with fewer custom components that could be accommodated in all APS SR ID locations. Many design details from the first generation cryostats were retained or only slightly modified to ease assembly and reduce cost. The primary requirement of zero boil-off operation was preserved although considerable commissioning activity has been required to achieve desired performance. Continued testing with the undulator magnet installed will be necessary to validate the cooling system and confirm that the magnet design meets the field specification. System response to a magnet quench was simulated using heaters and results were reasonably well aligned with predictions.

References

[1] Hasse Q, Fuerst J, Ivanyushenkov Y, Doose C, Kasa M, Shiroyanagi Y, Trakhtenberg E and Skiadopoulos D 2014 *Advances in Cryogenic Engineering* **1573 59A** 392.
[2] Fuerst J, Doose C, Hasse Q, Ivanyushenkov Y, Kasa M and Shiroyanagi Y 2014 *Advances in Cryogenic Engineering* **1573 59B** 1527.
[3] Bekhtenev E, Khruschev S, Kuper E, Lev V, Mezentsev N, Miginsky E, Repkov V, Shkaruba B, Syrovatin V and Tsukanov V 2006 *Physics of Particles and Nuclei Letters* **3 Suppl. 1** S16.
[4] Shiroyanagi Y, Fuerst J, Hasse Q and Ivanyushenkov Y 2016 *Proceedings of NAPAC2016* 1064.

Acknowledgments

This work was supported by the U.S. Department of Energy, Office of Science, under Contract No. DE-AC02-06CH11357.